

Tractography of the Optic Radiation for Vision Sparing Epilepsy Surgery

Chantal Tax, Remco Duits, Bart ter Haar Romeny
and Anna Vilanova

Department of Biomedical Engineering
Eindhoven University of Technology
Eindhoven, the Netherlands

C.M.W.Tax@student.tue.nl,
{R.Duits, B.M.terHaarRomeny, A.Vilanova}@tue.nl

Pauly Ossenblok

Kempenhaeghe Epilepsy & Sleep Center
Heeze, the Netherlands

OssenblokP@kempenhaeghe.nl

Abstract - In case of refractory localized temporal lobe epilepsy the anterior part of the temporal lobe and parts of the mesial structures can be removed with epilepsy surgery. After anterior temporal lobe resection approximately 60 to 80% of the patients become seizure free. However, a visual field deficit in the upper quadrant of the visual field is a complication that arises due to disruption of the most anterior part of the optic radiation (Meyer's loop) in up to 100% of the cases. In case of a severe visual field deficit, patients are not allowed to drive anymore after surgery. In this study we tackle the difficult task of mapping the highly curved fibers of Meyer's loop to assist the neurosurgical planning. Tractography seeding is done by fMRI for the calcarine sulcus, and manual outlining of the lateral geniculate nucleus. The fibers of the central, upper and lower visual areas could be discriminated on their specific lengths and curvatures.

Index Terms: Tractography, epilepsy, Diffusion Tensor Imaging, visual tract, blindness.

I. INTRODUCTION

Epilepsy is a common neurological disorder that is characterized by seizures that are clinical events, mostly defined by their signs and symptoms. The frequency of epileptic seizures can vary from multiple seizures a day to less than once a year [16]. Temporal Lobe Epilepsy (TLE) is characterized by seizures originating in or primarily involving temporal lobe structures such as the hippocampus, amygdala, and parahippocampal gyrus. Epilepsy surgery is considered when patients still have seizures that influence their life intensely despite medication, and when the epilepsy is localized. In standard Anterior Temporal Lobe Resection (ATLR) 4.0 to 6.5 cm of the anterior temporal lobe and portions of the medial structures are resected, after which approximately 60 to 80% of the patients become seizure free [9]. The Netherlands is one of the few countries where standard resections are still performed, while in a tailored approach intraoperative monitoring can guide the extent of resection [15].

A Visual Field Deficit (VFD) in the upper quadrant of the visual field is a common complication that arises in up to 100% of the cases [11,13]. Part of the Optic Radiation (OR) that connects the Lateral Geniculate Nucleus (LGN) to the primary visual cortex (or V1) is disrupted since it is located in the resection area (figure 1a). In the case of complete visual

loss in an upper quadrant (complete quadrantanopsia), the patient is not allowed to drive anymore. Visual field defects contribute a great deal in the reduction of the quality of life in these patients [19]. Since there exists a large inter-subject variability in the anterior extent of the OR, assessing the risk of a VFD is complicated and therefore localizing and visualizing the optic radiation is useful [8,24].

On conventional Magnetic Resonance Imaging (MRI), the optic radiation can hardly be distinguished from surrounding white matter, therefore Diffusion Weighted MRI (DW MRI) tractography can be used. Several studies have been done that use Diffusion Tensor Imaging (DTI) to reconstruct the fibers of the OR [21,22,23,24,29,31]. However, difficulties in tractography arise because of the local strong curvature of the optic radiation, and other fiber bundles in its proximity [13].

It is well known that the visual system is retinotopically organized, i.e. neurons originating from different areas of the retina have their specific positions within the visual pathway. The central field and upper and lower quadrant of the peripheral field are represented in three bundles in the OR accordingly (central, posterior and anterior bundle or Meyer's loop respectively, see figure 1.b). Localization of these three bundles within the optic radiation could be useful in assessing whether both the Meyer's loop and the central bundle would be disrupted leading to a complete upper quadrantanopsia [13,21,30].

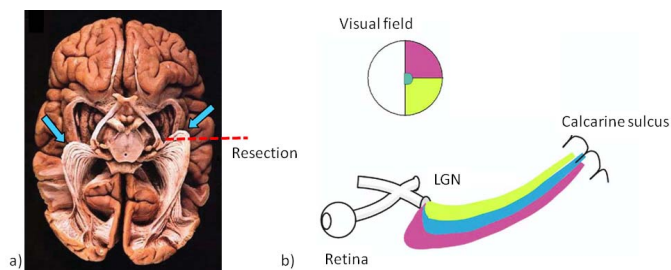


Fig. 1. a) The course of the OR, with the anterior part (Meyer's loop) extending in the temporal lobe, and thus often located in the resection area. b) Retinotopic organization of the visual system. (Figures adapted from [30])

II. METHODS

Two methods were developed to separate the three bundles of the optic radiation.

Method 1: The first one is based on the selective stimulation of the visual areas corresponding to the three bundles. For five healthy volunteers aged 21-26 an experiment was done to selectively stimulate the central field and upper and lower peripheral field. The stimuli presented were a full-field (FF), half-field (HF), upper quadrant (UQ) and lower-quadrant (LQ) as can be seen in figure 2. Experiments with different check sizes were done for different eccentricities based on the knowledge from literature on visual evoked potential (VEP) measured with electrodes on the scalp [3,17] and VEP combined with fMRI [4,26]. Dagnelie (1986) reports that the optimal element size of the square checkerboard pattern increases as the stimulus area moves outward, this corresponds to the linear increase of retinal receptive field size. For stimulation of the most central region, stimuli of 0-1° (6'), 0-2° (6' and 8'), 1-4° (16') and 0-4° (8' and 12') were used. To stimulate more peripheral, stimuli of 4-8° (15', 16', 20' and 28') were used. The Regions Of Interest (ROIs) were manually drawn based on the activity maps by placing a sphere with radius 6 mm at the center of the activity. The LGN was manually located on the T1 image and a sphere of 4 mm radius was placed as seed point. Fibers were tracked using the probabilistic ConTrack fiber tracking algorithm [20].

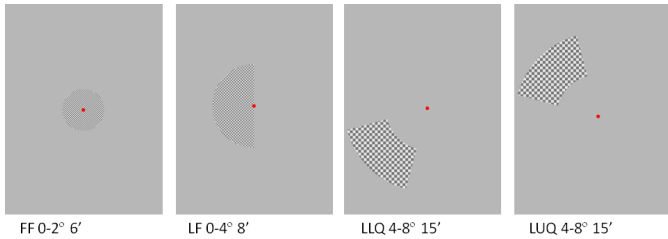


Fig. 2: Square checkerboard stimuli used in pattern onset experiments. 0-4° denotes the eccentricity angle, and 12' denotes the check size in arc minutes. The size of the red fixation point is 10'.

Method 2: An attempt is made to quantitatively separate the three bundles using an internal energy measure that takes into account the length and the curvature of the fibers. The internal energy of a curve is an energy measure that is defined by properties of the curve itself, not by any additional data. When keeping the purpose in mind (separation of three bundles) and looking at the anatomy of the OR known from literature [8], one could intuitively propose the following energy measure:

$$I(\gamma) = \int_0^{L_\gamma} \sqrt{\kappa^2(s) + \beta^2} ds$$

Where $I(\gamma)$ is the energy measure for pathway γ . Parameters s , $L_\gamma > 0$ and $\kappa(s)$ are respectively spatial arc length, total length and curvature of the curve. β is a parameter that can be tuned to punish or favor length. See also [3,5,6,7] for further reference. The anterior bundle first travels in the antero-lateral direction from the LGN and forms the Meyer's loop around the tip of the inferior horn, it then runs back and terminates around the lower lip of the calcarine sulcus in the occipital

lobe. This bundle would thus have the largest length and the most curvature. The central bundle starts laterally oriented, crosses the roof of the inferior horn and then runs to the pole of the occipital lobe. This bundle would thus have a smaller length and less curvature near the LGN. The posterior or upper bundle directly radiates posteriorly to the upper lip of the calcarine fissure. Curvature in each point can be calculated from the Frenet-Serret formulas analytically after cubic spline interpolation.

III. RESULTS

Method 1: Optimal activity was found for 0-2° 6', 0-4° 8' and 4-8° 15' or 16'. No activity was found for 0-1° at all. Figure 3 shows the activity maps projected on the inflated and flattened cortex for control 1. For subject 5 it was not possible to draw a seed region for the central bundle. The visus of the subjects was assumed to be good and therefore not tested, this could be an explanation. Figure 4a shows the OR as it could be constructed from manually drawing a seed region in V1 and the three bundles that result from fiber tracking using the ROIs drawn based on the activity maps for control 1. The table indicates how many highest scoring fibers remained for each bundle, and how many fibers still had to be manually removed since they were clearly no part of the OR. Figure b) represents the result on coronal slices at approximately the same locations as in the study of Ebeling and Reulen (1988) [8]. For this subject, the anterior and central bundle could successfully be reconstructed, the posterior bundle has some overlap with the central bundle.

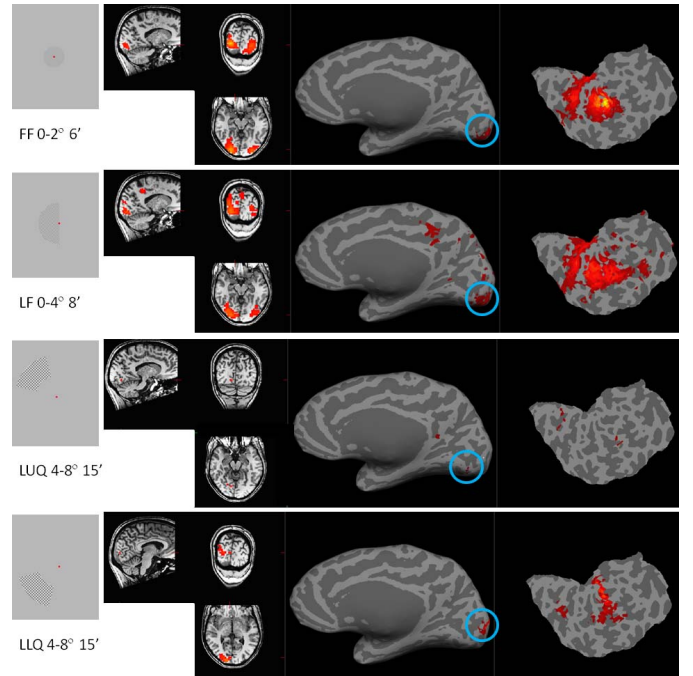
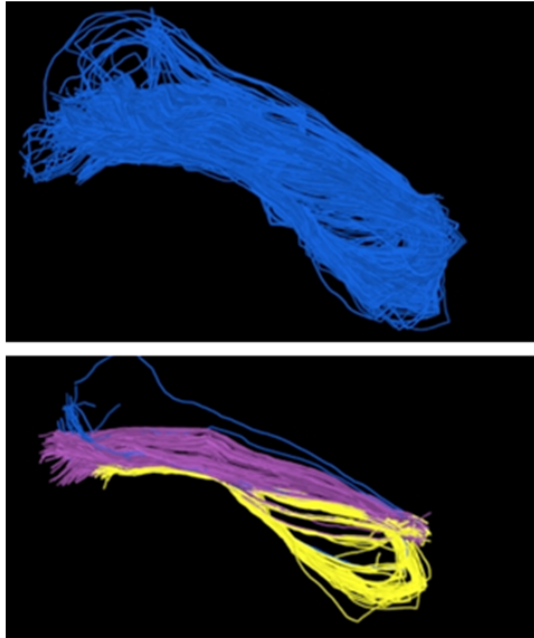


Fig. 3: Results for selective stimulation with new checkerboard stimuli (subject 1) FDR < 0.001, the blue circles indicate where the ROIs were drawn. For the remaining four control subjects, the results are summarized in figure 6. The top row shows the OR as it could be reconstructed by manually drawing the seed region in V1 and the LGN. Below the result of the reconstruction of the

three bundles is shown. For subject 2 and 4, the three bundles of the OR could be reconstructed. For subject 3 the posterior and central bundle could be separated, and in subject 5 the central bundle was not reconstructed since no seed point could be defined. For the anterior bundle of subject 2, a large amount of fibers not belonging to the OR had to be removed.



	Blue	Purple	Yellow
fibers	39	1348	476
removed	6	0	2

Fig. 4: Result of fiber tracking using three seed points based on the activity maps (subject 1), the anterior and central bundle could successfully be reconstructed, the posterior bundle has overlap with the central bundle.

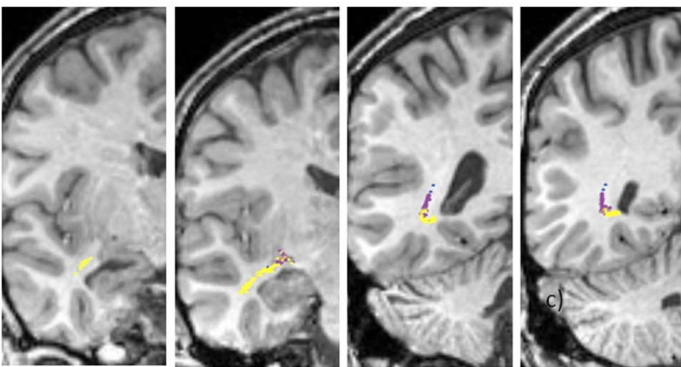


Fig. 5: Coronal slices with the position of the three bundles as in Ebeling and Reulen (1988) [7].

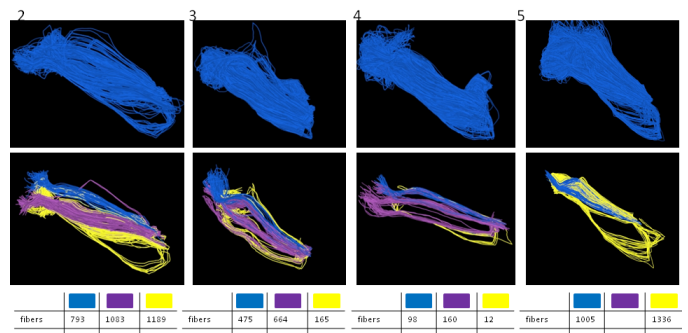


Fig. 6: Result of fiber tracking using three seedpoints based on the activity maps (subject 2-5).

Method 2: The result of calculating curvature per point can be seen in figure 7a. One can notice that curvature is calculated on a very fine scale, therefore a larger scale was used by down sampling the points along a fiber. Figure 7b shows that sampling up to every 12th point ($\Delta t = 12$) still gives plausible results. Because the difference in the three bundles occurs in the more anterior region of the OR, and the fibers fan out near to the calcarine sulcus, only the anterior half of the OR was used to calculate the internal energy. When the whole bundle was taken into account, no separation into three bundles could be obtained for this dataset. The histograms of the energy measure show three clusters for $\beta = 0.1$ or $\beta = 0.01$ and $\Delta t = 12$, and gives a visually plausible separation into three bundles, as can be seen in figure 8a for $\beta = 0.1$ and $\Delta t = 12$. The third cluster shows a wide range of energies. Figure 8b represents the result on coronal slices at approximately the same locations as in the study of Ebeling and Reulen (1988) [8]. The bundles do not seem to terminate clearly in the upper, central or lower region of the calcarine sulcus as would be expected from retinotopy.

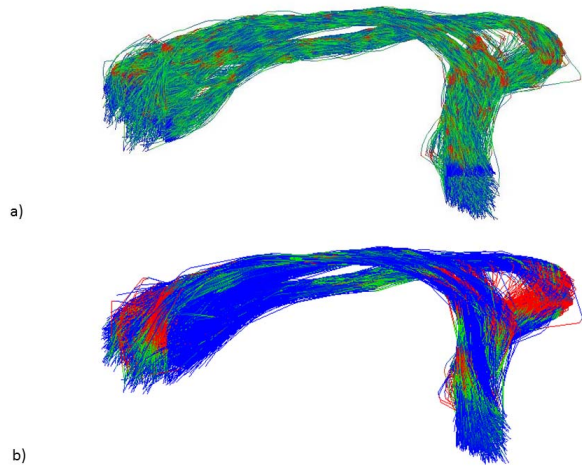


Fig. 7: a) Calculating curvature per point. b) Down sampling with $\Delta t = 12$ still yields plausible results.

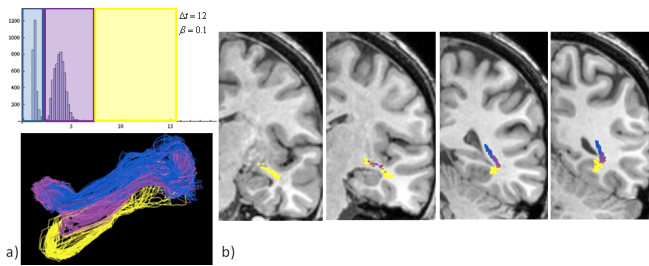


Fig. 8: a) Bundle separation using sample rate $\Delta t = 12$ and $\beta = 0.1$ and using thresholds $t_1 = 2.5$ and $t_2 = 7.5$.

IV. DISCUSSION

Stimuli were used to selectively stimulate the central field and upper- versus lower quadrant of the visual field. The check sizes increased approximately linearly when moving to periphery, corresponding to the linear increase of receptive field size in the retina. In all five subjects, BOLD activity was recognized in the lower and upper lip of the calcarine sulcus when stimulating with an upper- and lower quadrant peripheral stimulus respectively. In four out of five subjects activity was found on the occiput when stimulating with eccentricity $0-4^\circ$, and only for two subjects activity on the occiput could be located when using $0-2^\circ$.

One could wonder whether the spatial resolution of fMRI is sufficient to map these responses within V1. The width of the point spread function in V1 is approximately 3.5-3.9 mm at 3T [18], and the voxel size was 4 mm. The cortical magnification is large at the macula, and the value of 9.9 mm° [11] implies that the cortical area corresponding to the central stimulus is large enough compared to the spatial resolution of fMRI. However, difficulties measuring foveal activity with fMRI are well known [27], since fixation instability and the presence of the fixation marker interferes with measurements, and in many subjects there are large veins near these regions that introduce instrumental artifacts. Furthermore, the visus of the subjects was not tested. When stimulating peripheral with an upper quadrant stimulus, the activity indeed 'moves' anteriorly into the calcarine sulcus, as could be expected from retinotopy. It would be interesting to measure the distance of the activity to the occiput, and compare to what is reported in literature for this particular eccentricity. In contrast, the activity that results from the lower quadrant stimulus does not seem to move into the calcarine sulcus, but instead remains close to the occiput. No clear explanation was found for this observation.

In three out of five subjects, the bundles tracked from the selective seed regions did indeed seem to represent the posterior, central and anterior bundle when comparing the retinotopic organization on coronal slices with the study of Ebeling and Reulen (1988) [8]. In four out of five subjects, the posterior and central bundle could successfully be distinguished. The overall problem seems to be that the reconstruction of the anterior bundle overlaps the other bundles. This could be explained by the fact that the fiber tracking algorithm is not "sensitive" enough, and that the fiber propagation of the anterior bundle deviates into another bundle. Another explanation could be that the sphere of radius

6 mm was simply too large and not selective enough. However, additional experiments using a seed point with radius 4 mm did not improve the result. Additionally, fMRI as it is used in this project might not be accurate enough to locate these responses, which has resulted in a wrong placement of the seed points.

The linear relationship of the check sizes and eccentricity was chosen based on previous knowledge, tuning in some experiments, and in analogy with Di Russo (2002) [4]. It is known that V1 constitutes spatial frequency (SF) selectivity, and thus has maximal fMRI responses at particular spatial locations in V1 as in Henriksson (2008) [9]. The stimuli used in the article are substantially different from the stimuli used in this project, and the SF tuning curves are given in cycles° . It is hard to compare whether the spatial frequencies used in this project (i.e. the check sizes) correspond to maxima in the SF tuning curves generated in these articles. Tuning curves for these square checkerboard stimuli can be found in Dagnelie (1968) [3] for visual evoked potentials (VEPs) in monkey and in Ossenkop (1994) [17] for humans. Further research has to be done to fully optimize the check sizes at different eccentricities for fMRI, especially for eccentricities larger than 8° which were not used in this research.

Additionally, an internal energy approach was used to separate the three bundles. Each bundle was assigned an "energy" that depends on the total length of the fiber and the curvature along the fiber. In this way, a separation was expected of the Meyer's loop that is the longest and has the strongest curvature, the central bundle that is shorter and has less curvature, and the posterior bundle that runs straight back to the occipital pole. This method was tested for six "normal" optic radiations (one healthy control, and in patients prior to surgery or in the healthy hemisphere after surgery).

In all cases, the histograms of the energy showed three clusters when using $\beta = 0.1$ and a down sampling of $\Delta t = 10$ or 12. In five cases, this indeed resulted in a plausible separation of the three bundles. In two of these cases (one control and one preoperative patient), the retinotopic mapping on coronal slices was compared with the study of Ebeling and Reulen (1988) [8], which indicates that the bundles found could indeed correspond to the bundles of the OR. In none of the cases the bundles seemed to terminate in the lower or upper lip, or in the calcarine sulcus as would be expected from retinotopy.

This supports the thought of previous section that fiber tracking is not "sensitive" enough, since it seems that the tracking deviates into other bundles. Another explanation could be the mismatch of approximately 5 mm between the location of the neuronal and hemodynamic response. In future work this should be repeated for more "normal" optic radiations, to see whether fibers of the three bundles have typical internal energies. This could be compared with the results of bundle separation upon selective visual stimulation. However, differences in sizes of the brain and the OR between subjects have to be taken into account.

REFERENCES

- [1] X. Chen, D. Weigel, O. Ganslandt, M. Buchfelder, and C. Nimsky. Prediction of visual field deficits by diffusion tensor imaging in temporal lobe epilepsy surgery. *NeuroImage*, 45:286–297, 2009.
- [2] G. Dagnelie. Pattern and motion processing in primate visual cortex. PhD thesis, University of Amsterdam, 1986.
- [3] E.J. Creusen, R. Duits, and T.C.J. Dela Haije, Numerical Schemes for Linear and Non-linear Enhancement of DW-MRI, Lecture Notes in Computer Science, vol. 6667, 27-40, 2011.
- [4] F. Di Russo, A. Martinez, M. Sereno, S. Pitzalis, and S.A. Hillyard. Cortical sources of the early components of the visual evoked potential. *Human Brain Mapping*, 15:95–111, 2001.
- [5] R. Duits and E.M. Franken, Left-invariant Diffusions on the Space of Positions and Orientations and their Application to Crossing-preserving Smoothing of HARDI images. *International Journal of Computer Vision*, 92-3, 231-264, 2011,
- [6] R. Duits, T.C.J. Dela Haije, A. Ghosh, E.J. Creusen, A. Vilanova and B.M. ter Haar Romeny, Enhancement of DW-MRI, Lecture Notes in Computer Science, Springer, vol. 6667, 1-13, 2011.
- [7] R. Duits, E.J. Creusen, A. Ghosh, and T.C.J. Dela Haije, Diffusion, convection and erosion on $SE(3) \times SO(2)$ and their application to the enhancement of crossing fibers. ArXiv, March 2011, URL: arxiv.org/abs/1103.0656v5.
- [8] H.J. Reulen and Ebeling U. Neurosurgical topography of the optic radiation in the temporal lobe. *Acta Neurochirurgica*, 92:29–36, 1988.
- [9] J. Engel, et al. Early surgical therapy for drug-resistant temporal lobe epilepsy: a randomized trial. Early Randomized Surgical Epilepsy Trial (ERSET) Study Group. *JAMA*. 307(9):922–30, 2012
- [10] L. Henriksson, L. Nurminen, A. Hyvrinen, and S. Vanni. Spatial frequency tuning in human retinotopic visual areas. *Journal of Vision*, 80(10):1–13, 2008.
- [11] J.C. Horton and W.F. Hoyt. The representation of the visual field in human striate cortex, a revision of the classic holmes map. *Arch Ophthalmol*, 109:1–15, 2005.
- [12] T.S. Hughes, B. Abou Khalil, P.J. Lavin, T. Fakhoury, B. Blumenkopf, and S.P. Donahue. Visual field defects after temporal lobe resection: a prospective quantitative analysis. *Neurology*, 53(1):167–172, 1999.
- [13] C. Jacobs. A feasibility study to reconstruct the optic radiation for epilepsy surgery using fmri-seeded DTI tractography. Master's thesis, University of Technology Eindhoven, 2010.
- [14] P. Krolak-Salmon, M. Guenot, C. Tiliket, J. Isnard, M. Sindou, F. Mauguere, and A. Vighetto. Anatomy of optic nerve radiations as assessed by static perimetry and MRI after tailored temporal lobectomy. *Br J Ophthalmol*, 84:884–889, 2000.
- [15] R.I. Kuzniecky and G.D. Jackson. *Magnetic Resonance in Epilepsy: Neuroimaging Techniques*. Academic Pr, 2004.
- [16] Lüders. H.O. and Noachtar, *Epileptic Seizures Pathophysiology and clinical semiology*, S. Churchil Livingstone Philadelphia, 2000.
- [17] P. Ossenblok, D. Reits, and H. Spekreijse. Check size dependency of the sources of the hemifield onset evoked potential. *Ophthalmologica*, 88:77–88, 1994.
- [18] L.M. Parkes, J.V. Schwarzback, A.A. Bouts, R.R. Deckers, P. Pullens, C.M. Kerskens, and D.G. Norris. Quantifying the spatial resolution of the gradient echo and spin echo bold response at 3 tesla. *Magnetic Resonance in Medicine*, 54:1465–1472, 2005.
- [19] V. Pathak-Ray, A. Ray, R. Walters, and R. Hatfield. Detection of visual field defects in patients after anterior temporal lobectomy for mesial temporal sclerosis-establishing eligibility to drive. *Eye*, 16:744–748, 2002.
- [20] A.J. Sherbondy, R.F. Dougherty, M. Ben-Shachar, S. Napel, and B.A. Wandell. Contrack: Finding the most likely pathways between brain regions using diffusion tractography. *Journal of Vision*, 8:1–16, 2008.
- [21] A.J. Sherbondy, R.F. Dougherty, S. Napel, and Wandell B.A. Identifying the human optic radiation using diffusion imaging and fiber tractography. *Journal of Vision*, 8(10):1–11, 2008.
- [22] T. Taoka, et al. Diffusion tensor imaging in cases with visual field defect after anterior temporal lobectomy. *AJNR Am J Neuroradiol*, 26:797–803, 2005.
- [23] T. Taoka, M. Sakamoto, and H. Nakagawa. Diffusion tensor tractography of the Meyer loop in cases of temporal lobe resection for temporal lobe epilepsy: correlation between postsurgical visual field defect and anterior limit of Meyer's loop on tracto. *Am J Neuroradiol*, 29:1329–1334, 2008.
- [24] M.O. Thudium, A.R. Campos, H. Urbach, and H. Clusmann. The basal temporal approach for mesial temporal surgery: sparing the Meyer loop with navigated diffusion tensor tractography. *Neurosurgery*, 67:385–390, 2010.
- [25] S.G. Uijl, F.S.S. Leijten, J.B.A.M. Arends, J. Parra, A.C. van Huffelen, and K.G.M. Moons. Prognosis after temporal lobe epilepsy surgery: the value of combining predictors. *Epilepsia*, 49(8):1317–1323, 2008.
- [26] S. Vanni, J. Warnking, M. Dojat, C. Delon-Martin, J. Bullier, and C. Segebarth. Sequence of pattern onset responses in the human visual areas: an fMRI constrained VEP source analysis. *NeuroImage*, 21:801–817, 2004.
- [27] B.A. Wandell and J. Winawer. Imaging retinotopic maps in human brain. *Vision Res*, 51:718–737, 2011.
- [28] S. Wiebe, W.T. Blume, J.P. Girvin, and M. Eliasziw. A randomized, controlled trial of surgery for temporal-lobe epilepsy. *The New England Journal of Medicine*, 345(5):311–318, 2001.
- [29] A. Yamamoto, et al. Diffusion tensor fiber tractography of the optic radiation: analysis with 6-, 12-, 40-, and 81- directional motion-probing gradients, a preliminary study. *AJNR Am J Neuroradiol*, 28:92–96, 2007.
- [30] T. Yamamoto, K. Yamada, T. Nishimura, and S. Kinoshita. Tractography to depict three layers of visual field trajectories to the calcarine gyri. *Am J Ophthalmol*, 140:781–785, 2005.
- [31] M. Yogarajah, N.K. Focke, S. Bonelli, M. Cercignani, J. Acheson, G.J.M. Parker, D.C. Alexander, A.W. McEvoy, M.R. Symms, M.J. Koeppe, and J.S. Duncan. Defining Meyer's loop-temporal lobe resections, visual field deficits and diffusion tensor tractography. *Brain*, 132:1656–1668, 2009.